A role for ephrin-A5 in axonal sprouting, recovery, and activity-dependent plasticity after stroke

Justine J. Overman[a], Andrew N. Clarkson[b], Ina B. Wanner[c], William T. Overman[a], Ilya Eckstein[a], Jaime L. Maguire[d], Ivo D. Dinov[a], Arthur W. Toga[a], and S. Thomas Carmichael[a,1]

[a]Department of Neurology, David Geffen School of Medicine, and [c]Multiple Myeloma Research Consortium, Semel Institute for Neuroscience and Human Behavior, University of California, Los Angeles, CA 90095; [b]Departments of Anatomy and Psychology, University of Otago, Dunedin 9054, New Zealand; and [d]Department of Neuroscience, Tufts University School of Medicine, Medford, MA 02155

Edited by Anders Bjorklund, Lund University, Lund, Sweden, and approved June 29, 2012 (received for review March 13, 2012)

Stroke causes loss of neurological function. Recovery after stroke is facilitated by forced use of the affected limb and is associated with sprouting of new connections, a process that is sharply confined in the adult brain. We show that ephrin-A5 is induced in reactive astrocytes in periinfarct cortex and is an inhibitor of axonal sprouting and motor recovery in stroke. Blockade of ephrin-A5 signaling using a unique tissue delivery system induces the formation of a new pattern of axonal projections in motor, premotor, and prefrontal circuits and mediates recovery after stroke in the mouse through these new projections. Combined blockade of ephrin-A5 and forced use of the affected limb promote new and surprisingly widespread axonal projections within the entire cortical hemisphere ipsilateral to the stroke. These data indicate that stroke activates a newly described membrane-bound astrocyte growth inhibitor to limit neuroplasticity, activity-dependent axonal sprouting, and recovery in the adult.

cortical map | regeneration | repair | motor function | EphA4

Stroke is the leading cause of adult disability because of the brain's limited capacity for repair. Although some degree of spontaneous axonal sprouting occurs after stroke, the environment of the adult brain constrains axonal sprouting and the formation of new connections. Inhibitors of axonal growth in the adult have been described in CNS myelin, secreted from astrocytes near the stroke site, and in the expression of developmentally regulated axonal growth inhibitors, such as semaphorins and netrins (1). Blockade of myelin-associated axonal growth inhibitors produces axonal sprouting in connections after stroke (1). Although axonal sprouting in these connections has been correlated with functional recovery after stroke (1) and associated with changes in cortical sensory maps (2), the sprouting response or key system of connections that is necessary for recovery has not been determined.

Stroke induces a unique gene expression profile in sprouting neurons, or a sprouting transcriptome. This gene expression profile contains networks of integrated signaling systems that involve growth factors, cell surface receptors, intermediary cytoplasmic cascades, and transcription factor and epigenetic modulators of gene expression (3). We have shown in this sprouting transcriptome that stroke paradoxically activates axonal growth inhibitory molecules within sprouting neurons (3). Stroke activates an ephrinA receptor, EphA4, and molecules downstream from EphA4, including chimaerin-1. This suggests that in the adult brain, axonal sprouting is both induced by stroke and limited by a coinduction of receptors for growth cone collapse. We have previously found that ephrin-A5 is also up-regulated in the reorganizing cortex after stroke during the time period of axonal sprouting (4, 5). This raises the interesting possibility that stroke induces ephrinA growth inhibition in periinfarct tissue. Although the function of ephrinA signaling in tissue boundary formation and in spinal cord injury has been studied (6), there have been no studies of ephrinA signaling in glial scar formation, axonal sprouting, and recovery after stroke.

Here, we both induce and block ephrin-A5 signaling using pharmacological and genetic manipulations (Table 1) as well as clinically relevant methods of drug delivery to show that ephrin-A5 has a necessary role in normal functional recovery and activity-dependent plasticity in the adult mouse, that a locus of motor recovery after stroke lies within newly developed cortical circuits ipsilateral to the infarct, and that stroke produces a heightened activity-dependent axonal sprouting response in the adult mouse cortex that is also normally limited by ephrin-A5 signaling.

Results

Ephrin-A5 Is Induced in Reactive Astrocytes After Stroke. Ephrin-A5 can bind EphB2 and multiple EphA tyrosine kinase receptors (7). To identify the molecular anatomy of ephrin-A5 reactivation after stroke, we used laser capture microdissection to isolate reactive astrocytes (8) adjacent to the infarct (Fig. 1*A* and Fig. S1 *A*–*G*) after middle cerebral artery occlusion (MCAo) stroke during the time period of axonal sprouting (4, 5, 8). Stroke increases ephrin-A5 mRNA expression in reactive astrocytes 74-fold at day 7 after the infarct (73.7 ± 48.5-fold normalized to GAPDH expression in stroke astrocytes vs. control astrocytes) (Fig. 1*B*). In situ hybridization on day 14 after stroke showed that ephrin-A5 is induced in a broad region of periinfarct cortex, extending up to 3 mm away from the stroke (Fig. 1 *C* and *D*). EphrinA signals through binding and tyrosine phosphorylation of EphA receptors (7, 9). Stroke causes EphA receptor phosphorylation in a broad region of periinfarct cortex (Fig. 2*B*). Based on the results of measurement of mRNA in specific cell types, in situ hybridization to localize the mRNA expression to regions of pericortex, and Western blot analysis to quantify protein in cortical regions as a whole, stroke increases ephrin-A5 expression in reactive astrocytes and activates ephrin-A5 signaling within the region of poststroke axonal sprouting ipsilateral to the infarct (10, 11). This region corresponds to the location of sprouting neurons after stroke, which induce the ephrin-A5 receptor EphA4 (3).

Ephrin-A5 Blocks Neuronal Outgrowth in Vitro. The inhibitory effects of ephrin signaling on neurite outgrowth can be blocked by the soluble receptor decoy, EphA5-Fc (fragment, crystallizable) (12). Although ephrin-A5 can also bind other EphAs, such as EphA4, we selected EphA5-Fc as a primary receptor decoy

Author contributions: J.J.O. and S.T.C. designed research; J.J.O., A.N.C., I.B.W., J.L.M., and S.T.C. performed research; J.J.O., W.T.O., I.E., I.D.D., and A.W.T. contributed new reagents/analytic tools; J.J.O., A.N.C., W.T.O., and S.T.C. analyzed data; and J.J.O. and S.T.C. wrote the paper.

Conflict of interest statement: The authors received research funding from BioTime Inc. for a portion of these studies.

This article is a PNAS Direct Submission.

Freely available online through the PNAS open access option.

[1]To whom correspondence should be addressed. E-mail: scarmichael@mednet.ucla.edu.

See Author Summary on page 13154 (volume 109, number 33).

This article contains supporting information online at www.pnas.org/lookup/suppl/doi:10.1073/pnas.1204386109/-/DCSupplemental.

Table 1. Treatment and effect on ephrin signaling

Treatment	Effect
Ephrin-A5-Fc	Block ephrin signaling
EphA5-Fc	Block ephrin signaling
EphA4-Fc	Block ephrin signaling
Clustered ephrin-A5-Fc	Induce ephrin signaling
Fc control	No effect of ephrin signaling
Ephrin-A5 siRNA	Block ephrin signaling
Scrambled siRNA	No effect on ephrin signaling

because of EphA5 specificity; for example, EphA4 also binds with ephrinB class ligands. To test the functional effects of ephrin-A5 on axonal growth in cortical neurons, we used an in vitro measure of reactive astrocytosis (13). Ephrin-A5 levels increase in reactive astrocytes compared with control astrocytes (Fig. 1*E*). Outgrowth of cortical neurons on reactive astrocytes is inhibited vs. outgrowth on nonstretched astrocytes (Fig. 1 *F* and *G*). Neurite outgrowth is significantly greater on reactive astrocytes in the presence of EphA5-Fc (Fig. 1*H*). The total numbers of neurites per neuron (Fig. 1*I*) and neurite length per neuron (Fig. 1*J* and Fig. S1*H*) are significantly reduced on reactive astrocytes compared with nonstretched astrocytes ($P < 0.001$), but total neurites per neuron and neurite length return to control levels over reactive astrocytes with EphA5-Fc. Thus, reactive astrocyte growth inhibition can be blocked in vitro with EphA5-Fc in scar-like conditions.

Blockade of Ephrin-A5 After Stroke Produces New Patterns of Cortical Projections. To determine the effect of ephrin-A5 blockade on axonal sprouting in vivo, we used a model of stroke in the mouse somatosensory vibrissal cortex (barrel field) produced by branch vessel MCAo, in which axonal connections can be localized to functional brain regions. Mice received a stroke, followed 7 d later by delivery of EphA5-Fc or the Fc control. This time point for

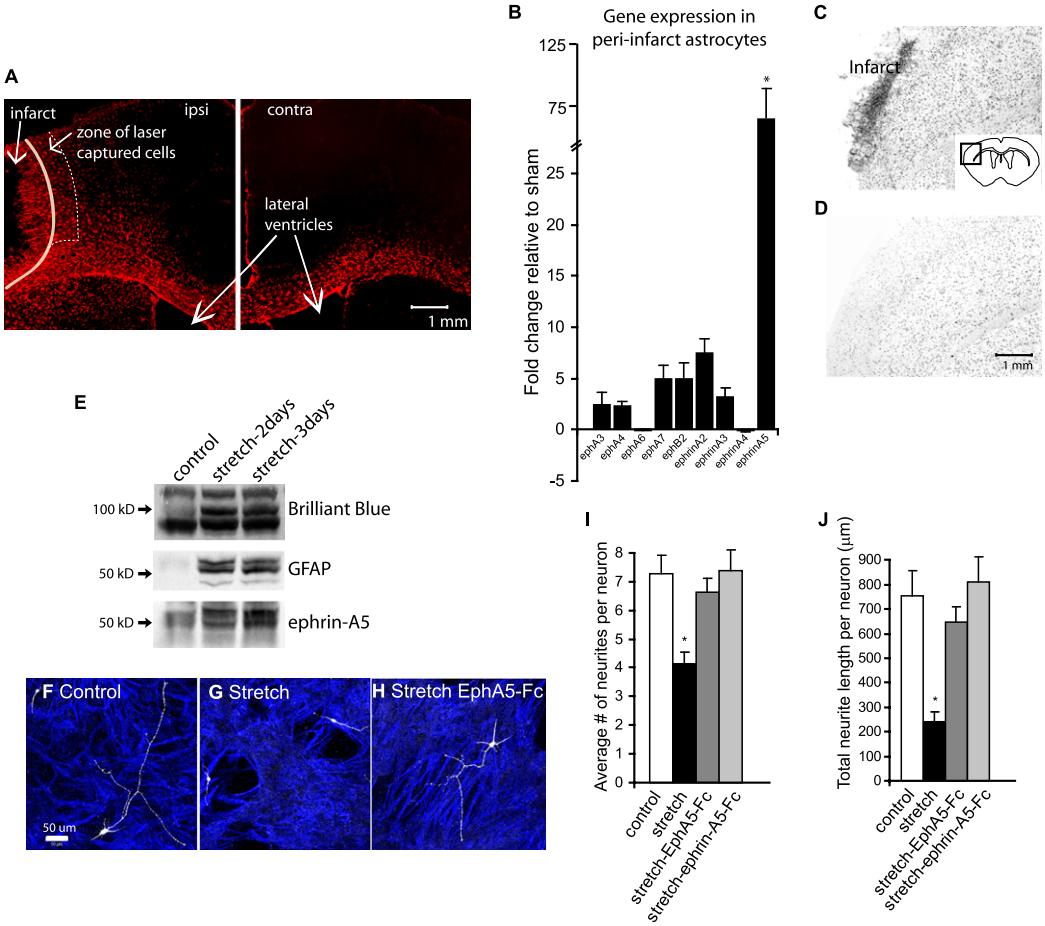

Fig. 1. Ephrin-A5 is up-regulated in astrocytes in periinfarct cortex. Ephrin-A5 signaling blockade results in improved neurite outgrowth on stretch-reactive astrocytes. (*A*) Laser capture microdissection of astrocytes in periinfarct cortex shows that ephrin-A5 is significantly up-regulated in astrocytes 7 d after stroke (*$P < 0.01$ by factorial ANOVA and Newman–Keuls' multiple pairwise comparisons for post hoc comparisons; $\alpha = 0.05$; $n = 3$). ipsi, ipsilateral; contra, contralateral. (*B*) Values are expressed as the fold change in the concentration ratio of gene expression after stroke normalized to GAPDH. In situ analysis of ephrin-A5 mRNA expression 14 d after stroke or sham operation shows increased ephrin-A5 expression in periinfarct cortex (*C*) compared with sham (*D*) ($n = 3$). (*E*) Western blot analysis shows that ephrin-A5 protein is increased in stretch-reactive astrocytes at 2 and 3 d poststretch compared with nonstretch control astrocytes in vitro. (*F–H*) Cortical neurons (β3 tubulin, white) from 9-d-old mice were seeded onto in vitro matured control (control) or stretch-reactive astrocytes (stretch) (GFAP, blue). Neuronal process regeneration is inhibited over stretched astrocytes (*G*) compared with controls (*F*). (*H*) Neurite outgrowth is more vigorous in the presence of EphA5-Fc on reactive astrocytes compared with reactive astrocytes alone. (*I*) Mean process number per neuron is reduced in neurons regenerating on stretched vs. control astrocytes ($P < 0.01$). Process number is increased in neurons on stretched astrocytes with EphA5-Fc (*$P < 0.05$; $n = 3$). Neurons on stretch-reactive astrocytes (stretch) alone have decreased outgrowth length to one-third of control lengths (control, *$P < 0.001$; $n = 3$). (*J*) EphA5-Fc improves neuron outgrowth on stretched astrocytes, reaching similar lengths as those on control astrocytes. Plotted are means (±SEM). *P* values in *I* and *J* were calculated using multiple comparison ANOVA with Tukey–Kramer post hoc analysis.

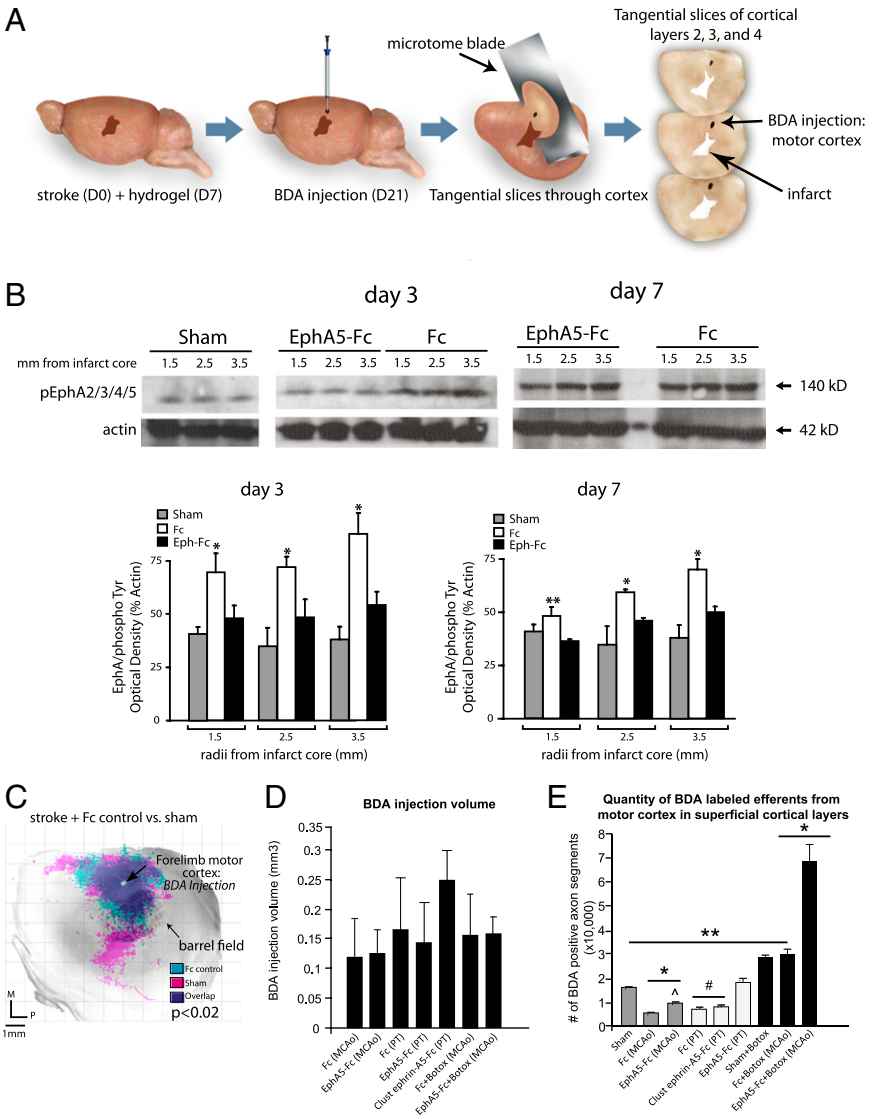

Fig. 2. Injection volume and quantity of labeled projections are uniform within groups, and EphA5-Fc blocks EphA phosphorylation. The techniques of stroke, hydrogel delivery of drug or vehicle, BDA (tracer) injection, and cortical flattening and tangential sectioning are illustrated. (*A*) Stroke is produced at day 0 (D0), hydrogel + drug is delivered to the infarct core at day 7 after stroke (D7), BDA is injected into the forelimb motor cortex at day 21 after stroke (D21), and tangential sections are cut through the flattened cortex. (*B*) Western blot analysis of phosphorylated EphA2/A3/A4/A5, normalized to actin, shows that levels of phosphorylated EphA (pEphA2/3/4/5) are lower in EphA5-Fc–treated animals at days 3 and 7 at 1.5, 2.5, and 3.5 mm from the infarct core compared with Fc control-treated animals and do not differ significantly from sham. phospho Tyr, phosphorylated tyrosine. (*C*) Projection map of sensorimotor cortex from labeled projections in sham-operated animals (pink), barrel field stroke + Fc control (turquoise), overlaid onto cytochrome oxidase-stained somatosensory body map. The BDA injection site is located at coordinates *x,y*: 0,0. (*D*) BDA injection volume is uniform within groups. (*E*) Total quantities of BDA-labeled 20-μm projection segments in the superficial layers of the cortex for each experimental group are plotted. For *B*, $*P < 0.05$ compared with EphA5-Fc and sham; $**P < 0.05$ compared with EphA5-Fc. For *E*, $*P < 0.001$ compared with sham; $\wedge P < 0.001$ compared with Fc (MCAo); $^{\#}P < 0.001$ compared with EphA5-Fc (PT); $**P < 0.001$ compared with EphA5-Fc + Botox (MCAo). Plotted in *B*, *D*, and *E* are means + SEM. *P* values were calculated by post hoc multiple pairwise comparison ANOVA, corrected for multiple comparisons using Tukey–Kramer post hoc analysis. M, medial; MCAo, barrel field stroke; P, posterior; PT, photothrombosis stroke.

drug delivery was chosen because it falls within the time frames of poststroke ephrin-A5 up-regulation and axonal sprouting (4, 5, 14). In addition, at 7 d poststroke, the microenvironment of the infarct core has stabilized a boundary of reactive astrocytes around the stroke cavity and implantation of hydrogel can be made without damage to adjacent tissue (15). Twenty-one days after stroke, microinjection of the tracer biotinylated dextran amine (BDA) was made into forelimb sensorimotor cortex, and animals were killed at 28 d after stroke (Fig. 2*A*). This time point corresponds to the point at which new patterns of axonal connections have been established and can be labeled (10). EphA5-Fc or Fc control was delivered via a biopolymer hydrogel placed into the infarct core. This hyaluronan/heparan sulfate hydrogel produces sustained local release of these molecules to the neighboring periinfarct cortex (3, 16) Fig. S2*A* Hydrogel implantation does not change the levels of astrocyte activation, neuronal survival, microglia or macrophage activation, or angiogenesis (Fig. S3). Delivery of EphA5-Fc at these concentrations via hydrogel effectively blocks ephrin signaling within periinfarct cortex, the target region for poststroke axonal sprouting (3) and an area associated with functional recovery (16, 17), as indicated by diminished EphA phosphorylation in periinfarct cortex (Fig. 2*B*).

To determine the effects of ephrin-A5 signaling on cortical projections after stroke in a rigorous manner, neuronal projections were mapped using a quantitative projection mapping system (3, 16). Neuronal projections in each mouse cortical hemisphere were plotted, mice were grouped by treatment condition, and cortical projection maps were then quantitatively compared across treatment groups using statistical tests for overall differences in cortical projections and for specific areas that have a different pattern of connections (Fig. 2*C* and Fig. S4 *A* and *B*). Neuronal sprouting is identified when a pattern of cortical projections is precisely mapped, by digital tracing of each BDA-labeled projection, and is statistically different across treatment conditions (3, 11). The connectional maps are then overlaid onto the underlying body maps produced by cytochrome oxidase staining to determine the cortical areas that exhibit changes in connections (Fig. 2*C*). All BDA injections (Fig. 2*D*) and infarct volumes (Fig. S5 *A–C*) were uniform across independent experimental conditions. The total number of BDA-labeled projections from motor cortex is reduced after stroke but is constant across stroke and control groups (Fig. 2*E*).

The registration of cortical projection maps with the underlying mouse somatosensory body map localizes projections to functional areas in the barrel field and adjacent cortical areas (Figs. 2*C* and 3*A*, *Inset*). Comparing motor cortex projections between sham and stroke mice, stroke causes a loss of somatosensory and long-distance (4 mm) premotor cortical projections (Fig. 2*C*). Stroke also causes a local increase in cortical projections within premotor and motor cortex close to forelimb motor cortex. Delivery of the receptor decoy EphA5-Fc to block ephrin signaling after stroke produces a significant increase in the number of motor cortex connections (Fig. 2*E*) and a pattern of cortical projections that is significantly different (Fig. 3*A*, red) from stroke + hydrogel with Fc control (Fig. 3*A*, light blue). In this new pattern of cortical connections, EphA5-Fc delivery after stroke produces a shift in the pattern of motor/premotor projections and new projections from motor cortex to prefrontal, somatosensory, and second somatosensory areas (Fig. 3*A*). This shift in projection outgrowth following ephrin-A5 signaling blockade with EphA5-Fc is also accompanied by an increase in the axon growth cone protein, GAP43 (Fig. S6*A*). Polar plots illustrating BDA-positive projection quantity and spatial distribution of projections show that these new patterns of projections from forelimb motor cortex to prefrontal, premotor, somatosensory, and second somatosensory areas are significantly different from stroke control and stroke + hydrogel Fc control (Fig. 3*B*). Polar plots are plotted in equivalent coordinates as cortical projection maps in Fig. 3*A*.

Ephin-A5 signaling is promiscuous and occurs through several EphA receptors. To understand the in vivo signaling systems that control poststroke axonal sprouting further, we manipulated additional receptor and ligand components in this system with an EphA4 receptor decoy and through directly knocking down ephrin-A5. EphA4-Fc delivery after stroke results in significant axonal sprouting within motor cortex, even compared with EphA5-Fc (Fig. 3*C* and Fig. S2*B*). In addition, there is an increase in the density of BDA-labeled projections in the premotor cortex region of interest (ROI) following delivery of EphA4-Fc compared with control (Fig. 3*E*). To pursue genetic knockdown of ephrin-A5 signaling, we used siRNA against ephrin-A5. This is because transgenic mice with KOs in ephrinAs or EphAs have an abnormal cortical organization, including abnormal cortical afferents, disturbed intracortical connections, and altered visual and somatosensory maps (18–21), making the analysis of rewiring in the adult brain after stroke compromised by profound developmental miswiring in cortex. Ephrin-A5 expression is knocked down by local delivery of ephrin-A5 siRNA (Fig. S2*D*), and this genetic knockdown produces a substantial increase in motor cortex projection distribution (Fig. 3*D* and Fig. S2*C*) and premotor cortex fiber density after stroke (Fig. 3*F*). In addition, delivery of ephrin-A5 siRNA results in increased expression of GAP43 (Fig. S2*F*).

These data indicate that stroke and ephrin-A5 blockade induce significant new connections within motor, premotor, and somatosensory cortical areas after stroke. We used two additional neuroanatomical techniques to define these new patterns of connections further. Lentivirus-GFP was used to label the anterograde projections emanating out from motor cortex after stroke, and the retrograde tracer cholera toxin B (CTb) subunit was used to back-label the neurons in motor cortex that project to premotor cortex after stroke; these are paired anterograde and retrograde studies in the same animal that can add to the BDA studies to reveal new patterns of connections directly. Following MCAo stroke, ephrin blockade with EphA5-Fc, and injection of lentivirus-GFP into the forelimb motor cortex and CTb into the premotor cortex (Fig. 4*A*), there is a significant increase in the premotor cortex GFP-positive fiber density (Fig. 4 *B* and *D*) and a change in the projection profile (Fig. 4*F*) compared with control (Fig. 4 *C* and *D*). There is also a significant increase in the density of CTb-positive cell bodies in motor cortex with axons that project to premotor cortex (Fig. 4 *B* and *E*) and a change in the distribution of cell bodies (Fig. 4*G*) following ephrinA blockade (Fig. 4*B*) compared with control (Fig. 4*C*). In summary, these anatomical data use three different tracing techniques, with both anterograde and retrograde or bidirectional labeling, to show that stroke plus ephrin-A5 blockade induces new motor, premotor, and somatosensory projections.

Ephrin-A5 Manipulations Control Motor Recovery After Stroke. We next tested whether the axonal sprouting after stroke that is stimulated with ephrin-A5 blockade induces functional recovery. To measure the function of these somatosensory, motor, and premotor circuits, we used a photothrombotic stroke model because the small barrel field strokes produced by branch vessel MCAo occlusion do not produce a consistent behavioral deficit (22). Photothrombotic stroke in the mouse forelimb motor cortex (23) produces consistent, long-lasting deficits in motor function, with a plateau in spontaneous recovery at day 42 (3, 17) (Fig. 5 *G* and *H* and Fig. S7*B*). EphA5-Fc delivery, beginning 7 d after photothrombotic stroke, induces a statistically significant increase in motor cortex connections (Fig. 2*E*) and a new pattern of projections (Fig. 5*A*) within motor, premotor, and somatosensory areas (Fig. 5*B*) in this photothrombotic stroke model, in the same brain regions in which new connections are seen with ephrinA blockade in the barrel cortex stroke model (Fig. 3*A*). There is also a significant increase in the density of BDA-positive projections in the premotor cortex after ephrin blockade compared with control (Fig. S7*A*). To quantify this axonal sprouting response in this stroke model further, we modified an approach from human brain mapping studies and analyzed each quantitative connectional map using a Student *t* test followed by regression analysis with post hoc false discovery rate correction for multiple comparisons within functional ROIs (24). ROIs were placed over premotor and somatosensory cortical areas (Fig. S6*B*), and the projections within these areas were statistically compared across all treatment groups. Delivery of EphA5-Fc results in a significantly different distribution of projections in the premotor cortex (Fig. 5*F*; $P < 0.05$, EphA5-Fc compared with Fc control). EphA5-Fc delivery after stroke also produces a statistically significant improvement in behavioral recovery of forelimb function after stroke (Fig. 5 *G* and *H*) that progressively develops over 8 wk after the infarct. Thus, EphA5-Fc induces axonal sprouting in sensorimotor cortical areas and a correlated behavioral recovery in motor function after stroke.

EphrinA signaling provides a unique opportunity to determine the system of projections necessary for behavioral recovery in stroke. Ephrin-A5 forward signaling to EphA receptors is me-

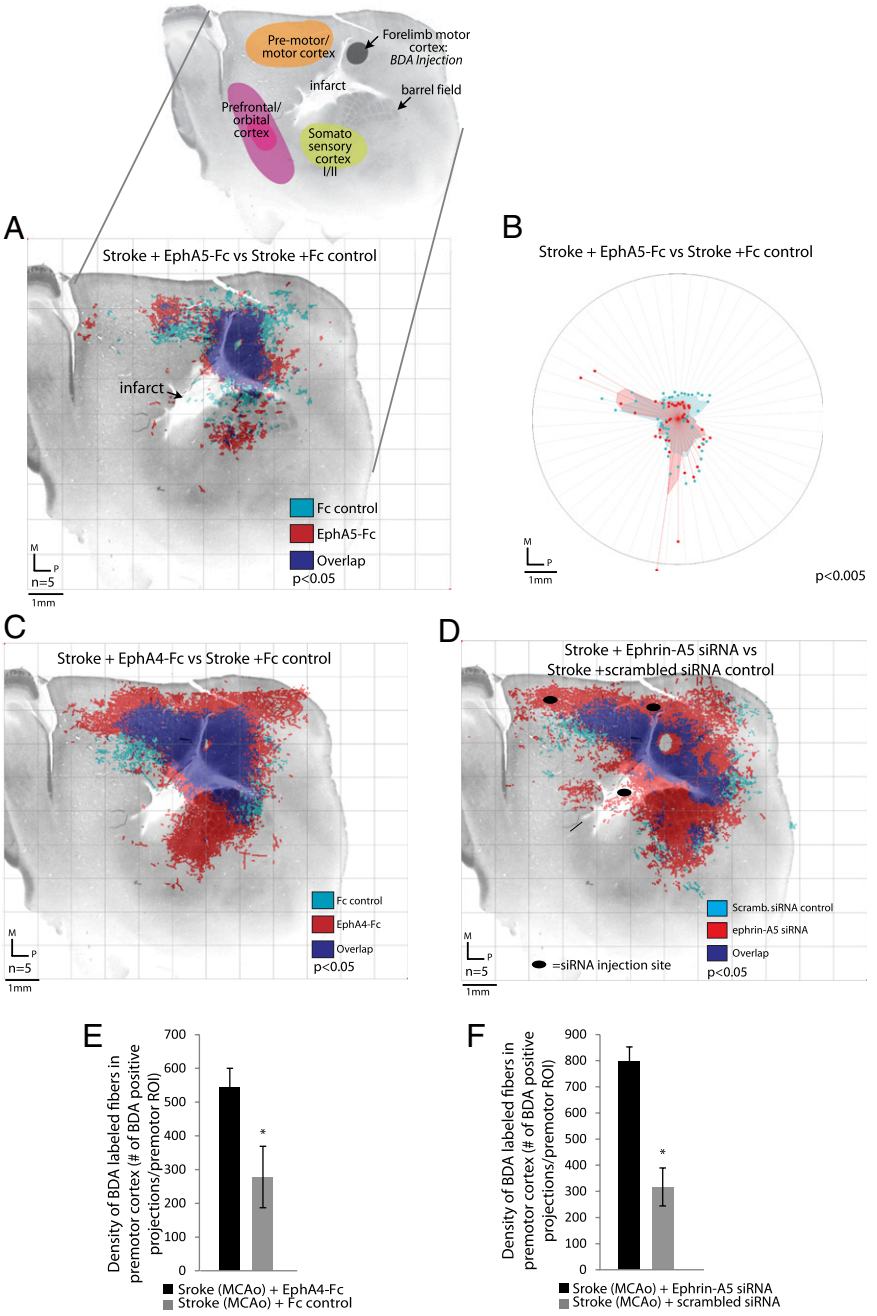

Fig. 3. Blockade of ephrin-A5 signaling leads to axonal sprouting in motor, premotor, and sensorimotor cortex. (*A*) Projection map of EphA5-Fc–treated animals (red) is significantly different from that of Fc control-treated animals (turquoise) (Hotelling's t^2 test; $P < 0.05$) following barrel field stroke. (*Inset*) Anatomical atlas of underlying cortical tissue, BDA injection, and barrel field stroke location. (*B*) Polar distribution map in register with connectional plot in *A* shows unique localization of sprouting in EphA5-Fc–treated animals compared with Fc control in regions of motor, premotor, and somatosensory cortex (Watson's U^2 test; $P < 0.005$). Shaded polygons represent the 70th percentile of the distances of labeled projections from the injection site in each segment of the graph; weighted polar vectors represent the normalized distribution of the quantity of points in a given segment of the graph for EphA5-Fc–treated (red) or Fc control (turquoise). (*C*) Projection map of EphA4-Fc–treated animals (red) is significantly different from that of Fc control-treated animals (turquoise) (Hotelling's t^2 test; $P < 0.05$). (*D*) Projection map of ephrin-A5 siRNA-treated animals (red) is significantly different from that of scrambled RNA control-treated animals (turquoise) (Hotelling's t^2 test; $P < 0.05$). Black ellipses in *D* indicate siRNA injection sites. (*E*) Density of BDA-labeled projections in premotor cortex is significantly greater in EphA4-Fc–treated animals compared with Fc control-treated animals (*$P < 0.05$, Student *t* test). (*F*) Density of BDA labeled projections in premotor cortex is significantly greater in ephrin-A5 siRNA-treated animals compared with scrambled siRNA control-treated animals (*$P < 0.05$, Student *t* test). $n = 5$ in all groups. M, medial; P, posterior.

diated by tetrameric or higher order cell surface EphA clustering (25, 26). This is blocked by the EphA5-Fc construct (27–30), as shown in the previous in vitro and in vivo studies. However, administering preclustered ephrin-A5-Fc will cluster EphA receptors, stimulate ephrin signaling, and mediate a gain of function in this growth inhibitory system within periinfarct cortex (7, 27, 29–31). Ephrin-A5-Fc was preclustered by incubation with anti-human IgG-Fc and delivered under the same protocol as EphA5-Fc in the photothrombotic stroke model. Clustered ephrin-A5-Fc results in the expected increased levels of phos-

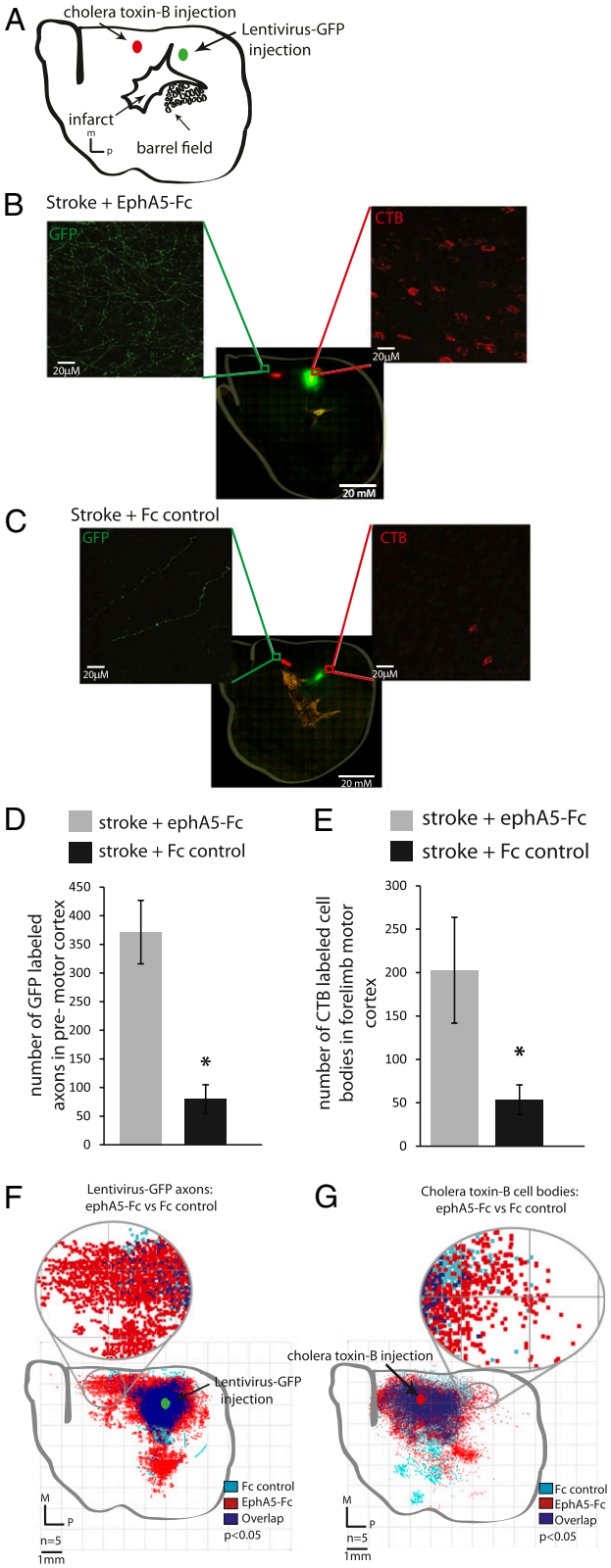

Fig. 4. Reciprocal labeling in motor and premotor cortex demonstrates new circuitry after stroke and ephrin blockade. (*A*) Animals received MCAo stroke, hydrogel + EphA5-Fc, or Fc control, followed by lentivirus-GFP injection into the forelimb motor cortex and CTb injection into the premotor cortex. High-magnification photomicrographs show representative images of GFP-positive axons (green) in premotor cortex and CTb-positive cell bodies (red) in motor cortex from EphA5-Fc–treated animals (*B*) and Fc control-treated animals (*C*). (*D*) There is a significantly greater density of GFP-positive axons in the premotor cortex in EphA5-Fc–treated animals compared with Fc control. (*E*) There is a significantly greater density of CTb-positive cell bodies in the motor cortex in EphA5-Fc–treated animals compared with Fc control. (*D* and *E*, *$P < 0.05$, Student's *t* test.) (*F*) Projection profile of anterogradely labeled GFP-positive axons is significantly different in EphA5-Fc–treated animals (red) compared with Fc control-treated animals (light blue) (Hotelling's t^2 test, $P < 0.05$). (*G*) Projection profile of retrogradely labeled CTb-positive cell bodies is significantly different in EphA5-Fc–treated animals (red) compared with Fc control-treated animals (light blue) (Hotelling's t^2 test, $P < 0.05$). $n = 5$ in all groups for *A*–*H*. M, medial; P, posterior.

phorylated Eph receptors 2, 3, 4, and 5 (Fig. S2*E*). Clustered ephrin-A5-Fc produces a significant block in the overall post-stroke axonal sprouting seen following treatment with EphA5-Fc (Fig. 5 *E* and *F*). Ephrin-A5 induction blocks the formation of new projections from motor cortex to prefrontal, premotor, and motor areas compared with ephrin-A5 signaling blockade after stroke (Fig. 5 *E* and *F*) and produces a pattern of cortical projections in prefrontal, premotor, and motor cortex that more closely resembles the stroke + Fc control condition (Fig. 5 *C* and *D*). Using ROI analysis, clustered ephrin-A5-Fc blocks axonal spouting from forelimb motor cortex to premotor cortex ($P < 0.05$, clustered ephrin-A5-Fc compared with EphA5-Fc; $P < 0.05$, clustered ephrin-A5-Fc compared with Fc control) and reduces sprouting in primary and secondary somatosensory cortex compared with EphA5-Fc ($P < 0.05$, clustered ephrin-A5-Fc compared with EphA5-Fc). However, sprouting in somatosensory cortex is not reduced to control levels ($P < 0.05$, clustered ephrin-A5-Fc compared with Fc control) (Fig. 6*F*).

Clustered ephrin-A5-Fc also blocks behavioral recovery. Fc control (vehicle-treated) mice show a slight recovery in limb control over 8 wk, and EphA5-Fc–treated mice show a significantly improved recovery across this time period (Fig. 5 *G* and *H*). However, mice with clustered ephrin-A5-Fc have forelimb and hind-limb control deficits that are significantly worse than both vehicle-treated and EphA5-Fc–treated animals (Fig. 5 *G* and *H* and Fig. S7*B*). Thus, induction of ephrin-A5 signaling blocks axonal sprouting in motor, premotor, and prefrontal circuits and reduces the normal recovery of motor function after stroke.

Ephrin-A5 Signaling Interacts with Patterned Behavioral Activity to Modulate Poststroke Cortical Reorganization. In patients who have had a stroke, forced use of the affected limb promotes recovery of that limb and remapping of brain activity in periinfarct cortex (32–34). If the ephrin-A5 system plays a significant role in remapping motor system projections within periinfarct cortex, it is important to test the interaction of ephrin-A5 signaling with forced limb use. Mice were forced to use their affected limb after stroke by administration of botulinum toxin (Botox) to the unaffected limb 24 h after stroke. This time point was chosen to maximize the patterned behavioral activity of the affected limb rather than to mimic clinical procedures. There is no effect on infarct size with this treatment (Fig. S5*B*). Overusing the affected forelimb in sham mice (Botox + nonstroke) produces a small but significant local increase in motor cortex projections compared with sham mice without Botox (Fig. 6*E*). Forced use after stroke (Botox + stroke/Fc control) induces a modest increase in projections from forelimb motor cortex into prefrontal and somatosensory areas compared with no forced use (no-Botox + stroke/Fc control) (Fig. 6*D*). However, forced use combined with EphA5-Fc administration (Botox + stroke/EphA5-Fc) induces a significant widespread increase in projections from the forelimb cortex throughout the cortical hemisphere ipsilateral to the infarct (Fig. 6 *A* and *B*). These new projections include an increased density of projections in premotor cortex (Fig. 6*C*) and striking new long-distance projections in frontal cortical regions that are virtually absent without ephrin-A5 blockade. Polar dis-

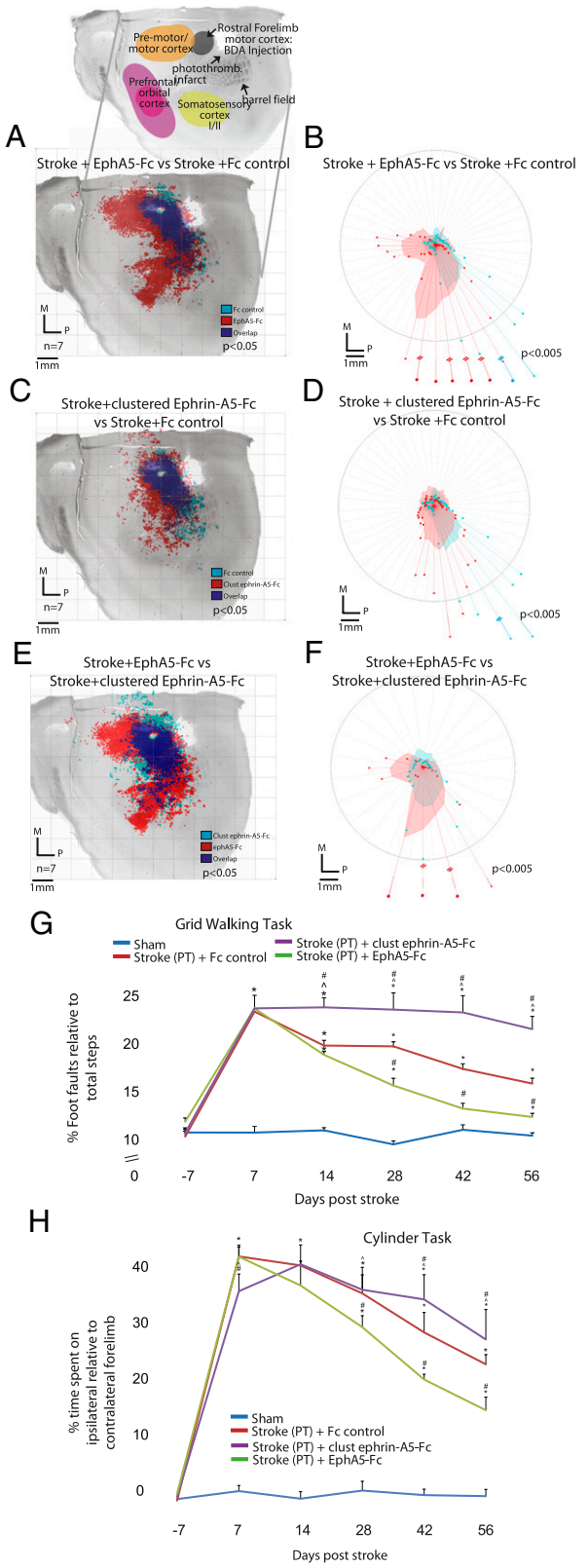

Fig. 5. Ephrin-A5 signaling regulates axonal sprouting and functional recovery after stroke. (*A*) Maps of projections from forelimb motor cortex in photothrombosis stroke for EphA5-Fc–treated animals (red) are significantly different from those for Fc control-treated animals (turquoise) (Hotelling's t^2 test, $P < 0.05$), with unique projections in motor, premotor, and somatosensory cortical areas. (*Inset*) Anatomical atlas of underlying cortical tissue, BDA injection, and photothrombotic stroke location. (*B*) Polar distribution maps indicate significantly different direction and magnitude of projections in EphA5-Fc–treated animals compared with control (Watson's U^2 test, $P < 0.005$). Clustered (Clust) ephrin-A5-Fc significantly blocks this axonal sprouting, producing a projection profile (Hotelling's t^2 test, $P < 0.01$) (*C*) and polar distribution (Watson's U^2 test, $P < 0.005$) (*D*), with an absence of axonal sprouting in motor and premotor cortex but not in somatosensory cortex compared with Fc control. A projection map (Hotelling's t^2 test, $P < 0.05$) (*E*) and polar distribution (Watson's U^2 test, $P < 0.005$) (*F*) of clustered ephrin-A5-Fc–treated animals are significantly different from those of EphA5-Fc–treated animals. There is an absence of axonal sprouting in premotor and prefrontal cortex and a reduction in somatosensory sprouting in clustered eprhin-A5-Fc–treated animals compared with EphA5-Fc–treated animals ($n = 7$). Units of axes are microns in A–*F*. EphA5-Fc–treated animals perform significantly better than control animals ($^{\#}P < 0.01$) on forelimb grid walking (*G*) and cylinder behavioral tasks (*H*). Behavioral recovery in animals following delivery of clustered ephrin-A5-Fc is significantly reduced compared with EphA5-Fc–treated ($\wedge P < 0.01$) and Fc control-treated ($^{\#}P < 0.01$) animals in grid-walking (*G*) and cylinder tasks (*H*). Plotted are means ± SEM. $n = 7$ in all groups. *P* values in *G* and *H* were calculated by post hoc multiple pairwise comparison repeated measures ANOVA, corrected for multiple comparisons using Tukey–Kramer post hoc analysis. clust, clustered; M, medial; P, posterior; PT, photothrombosis.

tribution maps (Fig. 6*B*; $P < 0.005$) and ROI analyses with multiple comparison corrections indicate that these projections are also significant in occipital/temporal and prefrontal/orbital cortex ($P < 0.05$, Botox + EphA5-Fc compared with Botox + Fc control) (Fig. 6*F*). Thus, stroke itself interacts with patterned behavioral activity to cause an increase in axonal sprouting in cortical areas related to sensorimotor representation of the overused limb; this sprouting is substantially increased to include much of the cortical hemisphere when ephrin-A5 signaling is blocked.

Discussion

Reactive astrocytes block axonal sprouting in stroke and other types of CNS injury. Astrocyte inhibitory molecules have previously been associated with secreted proteins, such as chondroitin sulfate proteoglycans (35). Data from single-cell laser capture, in vitro outgrowth assays, and in vivo blockade and induction of ephrin-A5 signaling in two different stroke models identify ephrin-A5 up-regulation in reactive astrocytes and show that ephrin-A5 inhibits axonal sprouting in cortical networks adjacent to the stroke that mediate motor recovery. A convincing study has described the inhibitory effects of myelin-based ephrin-B3 in spinal cord and optic nerve injury (36); however, the current study identifies ephrin-A5 in growth inhibition in the CNS after injury and assigns the cell type and functional role of this molecule in tissue reorganization and recovery after stroke. Functional recovery after stroke has been associated with axonal sprouting in several different brain connections, including corticocortical, corticospinal, and corticobulbar projections (37). Taking advantage of the ability not only to block ephrin-A5 signaling but to induce it, the present data show that axonal sprouting in motor, premotor, and prefrontal circuits in the cortex adjacent to the stroke is necessary for an enhancement in motor recovery after stroke in this mouse stroke model.

The ephrinA signaling system involves forward and reverse signaling through both ephrinA and EphA molecules and promiscuity in signaling between ephrinA and EphA members (7). Two elements of this ephrinA signaling promiscuity could play a role in stroke-induced axonal sprouting and recovery: the nature of the ephrinA ligand and the identity of the EphA receptor. Multiple ephrinA molecules other than ephrin-A5 may signal growth cone collapse and are present in astrocytes. Our data indicate that ephrin-A5 is the major molecular growth inhibitor. First, in a screen of the neuronal and astrocyte expression of EphA/ephrin molecules, eprhin-A5 mRNA expression is induced up to 70-fold in reactive astrocytes after stroke compared with

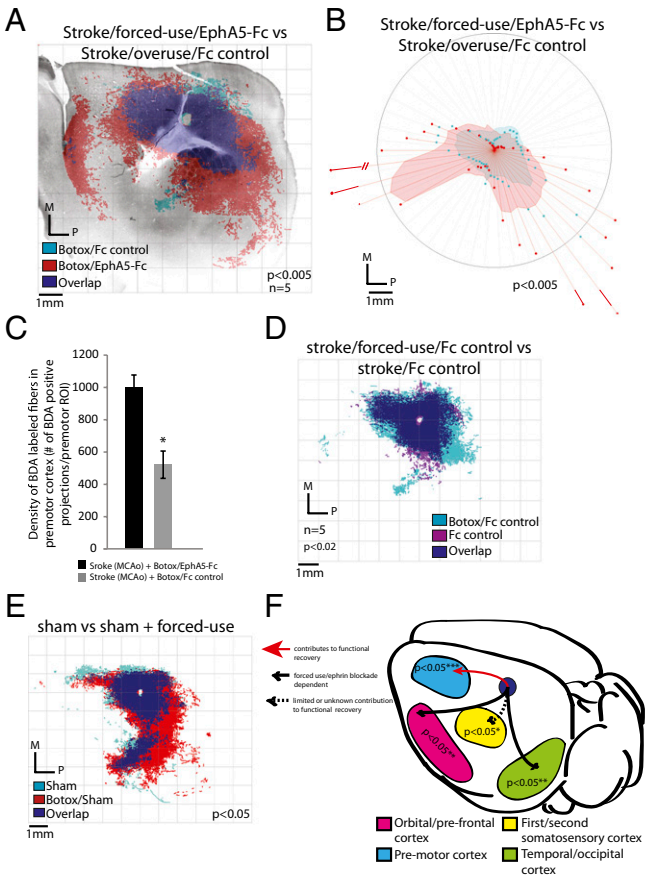

Fig. 6. Forced limb use combined with ephrin-A5 signaling blockade results in widespread reorganization of the ipsilateral cortex. (*A*) Composite map of forelimb motor cortex projections in Botox + EphA5-Fc stroke (red) and Botox + Fc stroke (blue) shows increase in motor cortex projections with Botox + EphA5-Fc (Hotelling's t^2 test, $P < 0.01$). (*B*) Polar distribution plot indicates that long-distance sprouting occurs in Botox + stroke/EphA5-Fc–treated animals (red) and is absent in Botox + stroke/Fc-treated animals (turquoise) (Watson's U^2 test, $P < 0.005$). (*C*) Density of BDA-labeled projections in premotor cortex in EphA5-Fc/Botox–treated animals is significantly greater than that of Fc control/Botox-treated animals (*$P < 0.05$, Student *t* test). (*D*) Composite map of Botox + Fc stroke (blue) compared with Fc stroke (no Botox, purple) indicates that there is a modest but significant difference in projections in Botox-treated stroke animals compared with non–Botox-treated stroke animals (Hotelling's t^2 test, $P < 0.02$). (*E*) Botox-induced restraint of the ipsilateral forelimb of sham-operated animals results in a significantly different projection profile compared with sham + no forced use (Hotelling's t^2 test, $P < 0.05$). $n = 5$ for all groups in *A*–*E*. (*F*) Student *t* tests and their corresponding *P* value maps were computed for each pixel of the projection map. Functionally relevant anatomical brain regions were defined as ROIs for statistical comparison across groups, and linear models were only fit over pixels covered by the ROI masks in premotor (blue), somatosensory I/II (yellow), prefrontal/orbital (pink), or temporal/occipital (green) cortical areas. The Student t^2 test, followed by an FDR post hoc ($a = 0.05$) analysis to correct for multiple comparisons, was applied at each pixel in the image domain to generate *P* values. Arrows and lines represent distinct functional networks induced by stroke, ephrin manipulation, and/or activity. Reported are significant differences ($P < 0.05$) between groups within the specified ROI. In *F*, ***$P < 0.05$ for MCAo EphA5-Fc vs. MCAo Fc control, PT EphA5-Fc vs. PT Fc control, and PT EphA5-Fc vs. PT clustered ephrin-A5-Fc; **$P < 0.05$ for MCAo EphA5-Fc + Botox vs. MCAo Fc control + Botox; *$P < 0.05$ for PT EphA5-Fc vs. PT Fc control.

other ephrinAs. Second, specific knockdown of ephrin-A5 with siRNA induces axonal sprouting after stroke. The identity of the EphA receptor for ephrin-A5 is less clear. Ephrin-A5 can signal through EphA2–EphA7 receptors (13). Blocking ephrinA signaling with both EphA4 and EphA5 decoys induces axonal sprouting; however, blockade with EphA4 produced the most robust sprouting response. There are a few possible explanations for why blockade with EphA4 produced the greatest sprouting response. First, EphA4 is induced in sprouting neurons after stroke (3) and may be the preferred binding partner for ephrin-A5 in this environment. Second, profiling of the entire sprouting transcriptome for sprouting neurons after stroke (3) also shows that chimaerin-1, a specific downstream Rho-GAP for EphA4 (38), is also induced in sprouting neurons. Finally, EphA4 is the only known ephrinA to interact with ephrinB class ligands (9). This cross-talk with ephrinB ligands may contribute to the differential sprouting response following delivery of ephA4-Fc compared with ephA5-Fc. However, because of the receptor/ligand promiscuity within the ephrinA family, reagents, such as EphA5-Fc and EphA4-Fc, will both interact with multiple EphA and ephrinA molecules. Thus, the specific EphA receptor may be EphA4 but cannot be definitively determined from these datasets.

The effect of clustering ephrin-A5-Fc to induce ephrin signaling indicates that ephrin-A5 normally limits axonal sprouting and behavioral recovery through forward signaling to neuronal EphA receptors. Our Western blot and in situ hybridization data show that this ephrin-A5 forward signaling activates EphA in a surprisingly broad area of periinfarct cortex, extending from the stroke site into virtually the entire ipsilateral mouse cortical hemisphere. Although reactive astrocytes cluster tightly near the infarct core, they can be found in decreasing numbers throughout the ipsilateral cortical hemisphere (39). These data indicate that although the hemisphere ipsilateral to the stroke appears morphologically intact and structurally "normal," a distributed population of reactive astrocytes locks down cortical projection systems through ephrin-A5 blockade.

Poststroke axonal sprouting has also been described from cortex contralateral to the stroke into cortical, brainstem, and spinal cord sites (40–42). The degree of axonal sprouting in these connections has been correlated with behavioral recovery and can be enhanced with Nogo blockade and inosine delivery (1, 43), but it has not been possible to block sprouting selectively in these circuits and to determine definitively their role in recovery. We used the ephrin-A5 system to both induce and block axonal sprouting and a hydrogel delivery system to influence molecular signaling selectively within periinfarct cortex, and we then assessed the patterns of connections in motor cortex circuits using three different neuroanatomical tracers with three statistical analysis measures. A new network of premotor, prefrontal, and motor projections, which was necessary for motor recovery, formed in cortex ipsilateral to the stroke (Fig. 6*F*). This was supported by ephrinA gain- and loss-of-function studies: Blocking ephrinA induces axonal sprouting and enhances functional recovery; inducing ephrinA blocks axonal sprouting and reduces or blocks motor recovery.

Forced use of the affected limb through constraint or motor skill learning after stroke has been shown to promote cortical remapping in periinfarct cortex in patients and promotes functional recovery in humans, nonhuman primates, and rats (32, 33). Using the detail provided by quantitative projection mapping, modest axonal sprouting was found within primary motor and sensory areas with forced use of the affected limb in control animals and following stroke alone. This provides a projection map to the ultrastructural reports of increased synapses in motor cortex with forced use of the forelimb (44, 45). A major finding in the present study is that there is a strong interaction of behavioral activity patterns with inhibitory cues after stroke to limit the extent of reorganization attributable to limb forced use. By blocking ephrin-A5 signaling, in conjunction with forced use, axonal sprouting and cortical reorganization are robust, and novel motor system projections are formed throughout the ip-

silateral cortical hemisphere (Fig. 6*F*). This degree of activity-dependent rewiring of frontal, lateral, and caudal somatosensory and temporal cortical circuits is unique to the combinatorial approach of forced use and blockade of ephrin-A5 signaling. Forced limb use in rodents activates a wide range of cortical areas beyond primary motor cortex (46) and induces neuronal growth factors in these areas (47). This distributed cortical activity pattern may play a role in the widespread cortical sprouting response following ephrin-A5 blockade and forced limb use after stroke.

The present data show that astrocytic ephrin-A5 limits sprouting from cortical neurons, is up-regulated after stroke, blocks axonal sprouting in premotor-prefrontal motor circuits, and limits motor recovery after stroke. Using a clinically relevant method of drug delivery, ephrin-A5 signaling can be blocked, new connections are formed, and functional recovery improves. The overall time course and persistence of these new connections in the lifetime of the animal after stroke remain to be determined. Also, it is likely that other cortical systems and distinct molecular signals within these systems play a role in the larger context of behavioral recovery after stroke. These molecular systems may include myelin inhibitors (NogoA), cytokines, and inducers of specific serine/threonine kinases (35, 48, 49). Pharmacological targets for post-stroke neural repair will result from further identification of the axonal sprouting control points in the adult, as well as the development of delivery systems to modulate these control points in a specific and local manner.

Materials and Methods

Surgical Procedures. Focal branch artery MCAo produces a barrel field stroke, which was generated on 2- to 4-mo-old adult mice (C56B/6; Charles River Laboratories) as described (22). For behavioral studies, focal cerebral ischemia was induced by photothrombosis [anterior/posterior (AP): 0 and medial/lateral (ML): 1.5] in male mice weighing 20–25 g as previously described (23). A hyaluronan/heparin sulfate proteoglycan biopolymer hydrogel (Glycosan HyStem-HP; BioTime, Inc.) was used to deliver EphA5-Fc, EphA4-Fc, human IgG-Fc (vehicle and antibody control), or preclustered ephrin-A5-Fc locally to the periinfarct cortex (3, 16).

After 21 d, animals received an injection of 10% (wt/vol) BDA (10,000 molecular weight; Invitrogen) into the forelimb motor cortex for the barrel cortex stroke or into the rostral border of the forelimb motor cortex for the photothrombotic stroke. In one experiment, lentivirus-GFP (phosphoglycerate kinase promoter; University of California, Los Angeles Vector Core) was injected into the forelimb motor cortex instead of BDA, and the retrograde tracer CTb (C-22842; Molecular Probes) was injected into the premotor cortex (anterior/posterior: 2.5, medial/lateral: 1.5, and dorsal/ventral: 0.75). For the forced-use studies, a volume of 0.15 μL Botox diluted 1:7 was injected into five areas 24 h after stroke, with 0.03 μL administered i.m. at each site: extensor and flexor compartments of the forelimb, biceps, triceps, and deltoid muscles to induce muscle paresis.

Laser Capture Microdissection. Brain sections were immunohistochemically stained for NeuN to label adult neurons and for GFAP to label astrocytes. One hundred fifty to 200 NeuN- or GFAP-positive cells were laser-captured (Veritas System; Molecular Devices) per brain, and total RNA was extracted from isolated cells with the RNAeasy Micro isolation kit (Qiagen) according to the manufacturer's protocol. cDNA was synthesized from equal amounts of RNA (150 ng). Samples were quantified by TaqMan real-time quantitative PCR (Applied Biosystems) using probe/primer sets for the expression of GAPDH as a baseline control and ephrinAs and the binding partners for ephrin-A5 (Table S1).

In Vitro Neurite Outgrowth Experiments. Reactive axonal growth-inhibitory astrocytes are obtained by maturing cortical astrocytes on deformable collagenated membranes for 4 wk and subsequently traumatizing them mechanically using an abrupt 3.4-psi pressure pulse with a pneumatic device as previously described (13). Cortical neurons from 9-d-old mice were isolated and cocultured for 24 h with prior stretched or unstretched astrocytes as reported (13). Stretch-conditioned, serum-free medium was supplemented with 15 μg/mL EphA5-Fc chimera. Images of regenerating neurons from each culture were taken using a confocal microscope (Zeiss LSM510; Carl Zeiss MicroImaging, Inc.), and neurites were traced blinded to treatment using a Neurolucida/Neuroexplorer (Microbrightfield). Total neurite length per neuron and number of neurites were compared.

Histology. At 28 d poststroke, animals were perfused with 0.1 M PBS followed by 4% (wt/vol) paraformaldehyde, and 40 μm tangential cortical sections were sliced using a sliding microtome. Sections were processed for cytochrome oxidase histochemistry to visualize the somatosensory body map, as previously described (50). BDA was visualized in the same sections (10, 51) using the Standard Vectastain Elite Kit (Vector Labs) and the chromogen diaminobenzamidine enhanced with cobalt chloride.

Quantification of Axonal Sprouting. Axonal sprouting was quantified as previously described (3, 16). Briefly, axonal sprouting was quantified by digitally marking each BDA-positive process in the superficial layers of the cortex (layers 2/3 and 4) from five animals per group. BDA-positive processes were marked *x/y* coordinates relative to the center of the injection site by an observer blinded to the treatment conditions, producing a Cartesian map of brain connections. Maps thus represent digitally traced replicas of the BDA-labeled projection raw data, have very little within-group variability, and have negligible changes attributable to time of tissue processing (Fig. S4 and Table S2). The *x/y* axonal plots from each brain were registered with respect to the injection site and coregistered with functionally relevant anatomical regions, produced by the staining of the mouse somatosensory body map in cytochrome oxidase, to generate a composite projection map for each treatment condition. Individual brain maps were then registered into composite maps per experimental condition. These maps were then analyzed for statistically significant differences in connectional profiles between groups utilizing three different analysis paradigms using three different approaches, which are described in detail in *SI Materials and Methods*.

Behavioral Assessment. Recovery of forelimb motor function was assessed using two well-characterized behavioral measures (17). Animals were tested once on both the grid-walking and cylinder tasks 1 wk before surgery to establish baseline performance levels and were then tested weekly out to 8 wk post-insult. Behaviors were scored by observers, who were blinded to the treatment group of animals in the study, from a high-speed videotape of each animal. Descriptions of additional methods, including detailed methodology for laser capture microdissection, in situ hybridization, neurite outgrowth on stretch reactive astrocytes, Western blot analysis, and behavioral testing, can be found in *SI Materials and Methods*.

ACKNOWLEDGMENTS. We thank Michal Machnicki, Shana Kalaria, Jesse Brown, Ellen Walker, and Russel Early for their technical assistance and Jean DeVellis for use of the Intellectual and Developmental Disabilities Research Center imaging core facility. This research was funded by National Institutes of Health Grants NS045729, NS061530-02 NS049041, National Science Foundation Division of Undergraduate Education 0716055, K99-NR010797, and RR021813; Neilsen Foundation Grant 20080654: 59240; the Larry L. Hillblom Foundation; and the Dr. Miriam and Sheldon G. Adelson Medical Research Foundation.

1. Lee JK, Kim JE, Sivula M, Strittmatter SM (2004) Nogo receptor antagonism promotes stroke recovery by enhancing axonal plasticity. *J Neurosci* 24:6209–6217.
2. Brown CE, Aminoltejari K, Erb H, Winship IR, Murphy TH (2009) In vivo voltage-sensitive dye imaging in adult mice reveals that somatosensory maps lost to stroke are replaced over weeks by new structural and functional circuits with prolonged modes of activation within both the peri-infarct zone and distant sites. *J Neurosci* 29: 1719–1734.
3. Li S, et al. (2010) An age-related sprouting transcriptome provides molecular control of axonal sprouting after stroke. *Nat Neurosci* 13:1496–1504.
4. Li S, Carmichael ST (2006) Growth-associated gene and protein expression in the region of axonal sprouting in the aged brain after stroke. *Neurobiol Dis* 23:362–373.
5. Carmichael ST, et al. (2005) Growth-associated gene expression after stroke: Evidence for a growth-promoting region in peri-infarct cortex. *Exp Neurol* 193:291–311.
6. Goldshmit Y, et al. (2011) EphA4 blockers promote axonal regeneration and functional recovery following spinal cord injury in mice. *PLoS ONE* 6:e24636.
7. Pasquale EB (2005) Eph receptor signalling casts a wide net on cell behaviour. *Nat Rev Mol Cell Biol* 6:462–475.
8. Burbach GJ, Dehn D, Nagel B, Del Turco D, Deller T (2004) Laser microdissection of immunolabeled astrocytes allows quantification of astrocytic gene expression. *J Neurosci Methods* 138:141–148.
9. Himanen JP, et al. (2004) Repelling class discrimination: Ephrin-A5 binds to and activates EphB2 receptor signaling. *Nat Neurosci* 7:501–509.

10. Carmichael ST, Wei L, Rovainen CM, Woolsey TA (2001) New patterns of intracortical projections after focal cortical stroke. *Neurobiol Dis* 8:910–922.
11. Dancause N, et al. (2005) Extensive cortical rewiring after brain injury. *J Neurosci* 25: 10167–10179.
12. Bolz J, et al. (2004) Multiple roles of ephrins during the formation of thalamocortical projections: Maps and more. *J Neurobiol* 59(1):82–94.
13. Wanner IB, et al. (2008) A new in vitro model of the glial scar inhibits axon growth. *Glia* 56:1691–1709.
14. Carmichael ST, Chesselet MF (2002) Synchronous neuronal activity is a signal for axonal sprouting after cortical lesions in the adult. *J Neurosci* 22:6062–6070.
15. Katsman D, Zheng J, Spinelli K, Carmichael ST (2003) Tissue microenvironments within functional cortical subdivisions adjacent to focal stroke. *J Cereb Blood Flow Metab* 23 (9):997–1009.
16. Clarkson AN, et al. (2011) AMPA receptor-induced local brain-derived neurotrophic factor signaling mediates motor recovery after stroke. *J Neurosci* 31:3766–3775.
17. Clarkson AN, Huang BS, Macisaac SE, Mody I, Carmichael ST (2010) Reducing excessive GABA-mediated tonic inhibition promotes functional recovery after stroke. *Nature* 468:305–309.
18. Cang J, et al. (2005) Ephrin-as guide the formation of functional maps in the visual cortex. *Neuron* 48:577–589.
19. Guellmar A, Rudolph J, Bolz J (2009) Structural alterations of spiny stellate cells in the somatosensory cortex in ephrin-A5-deficient mice. *J Comp Neurol* 517:645–654.
20. Uziel D, Mühlfriedel S, Bolz J (2008) Ephrin-A5 promotes the formation of terminal thalamocortical arbors. *Neuroreport* 19:877–881.
21. Uziel D, et al. (2002) Miswiring of limbic thalamocortical projections in the absence of ephrin-A5. *J Neurosci* 22:9352–9357.
22. Ohab JJ, Fleming S, Blesch A, Carmichael ST (2006) A neurovascular niche for neurogenesis after stroke. *J Neurosci* 26:13007–13016.
23. Lee SH, et al. (2004) Effects of hsp70.1 gene knockout on the mitochondrial apoptotic pathway after focal cerebral ischemia. *Stroke* 35:2195–2199.
24. Dinov IDVHJ, et al. (2009) Efficient, Distributed and Interactive Neuroimaging Data Analysis Using the LONI Pipeline. *Front Neuroinform* 3:22.
25. Himanen JP, Saha N, Nikolov DB (2007) Cell-cell signaling via Eph receptors and ephrins. *Curr Opin Cell Biol* 19:534–542.
26. Wimmer-Kleikamp SH, Janes PW, Squire A, Bastiaens PI, Lackmann M (2004) Recruitment of Eph receptors into signaling clusters does not require ephrin contact. *J Cell Biol* 164:661–666.
27. Davis S, et al. (1994) Ligands for EPH-related receptor tyrosine kinases that require membrane attachment or clustering for activity. *Science* 266:816–819.
28. Gerlai R, et al. (1999) Regulation of learning by EphA receptors: A protein targeting study. *J Neurosci* 19:9538–9549.
29. Kramer ER, et al. (2006) Cooperation between GDNF/Ret and ephrinA/EphA4 signals for motor-axon pathway selection in the limb. *Neuron* 50:35–47.
30. Stein E, et al. (1998) Eph receptors discriminate specific ligand oligomers to determine alternative signaling complexes, attachment, and assembly responses. *Genes Dev* 12: 667–678.
31. Lawrenson ID, et al. (2002) Ephrin-A5 induces rounding, blebbing and de-adhesion of EphA3-expressing 293T and melanoma cells by CrkII and Rho-mediated signalling. *J Cell Sci* 115:1059–1072.
32. Könönen M, et al. (2005) Increased perfusion in motor areas after constraint-induced movement therapy in chronic stroke: A single-photon emission computerized tomography study. *J Cereb Blood Flow Metab* 25:1668–1674.
33. Wolf SL, et al.; EXCITE Investigators (2006) Effect of constraint-induced movement therapy on upper extremity function 3 to 9 months after stroke: The EXCITE randomized clinical trial. *JAMA* 296:2095–2104.
34. Sawaki L, et al. (2008) Constraint-induced movement therapy results in increased motor map area in subjects 3 to 9 months after stroke. *Neurorehabil Neural Repair* 22: 505–513.
35. Yiu G, He Z (2006) Glial inhibition of CNS axon regeneration. *Nat Rev Neurosci* 7: 617–627.
36. Duffy P, et al. (2012) Myelin-derived ephrinB3 restricts axonal regeneration and recovery after adult CNS injury. *Proc Natl Acad Sci USA* 109:5063–5068.
37. Carmichael ST (2006) Cellular and molecular mechanisms of neural repair after stroke: Making waves. *Ann Neurol* 59:735–742.
38. Dalva MB (2007) There's more than one way to skin a chimaerin. *Neuron* 55:681–684.
39. Katsman D, Zheng J, Spinelli K, Carmichael ST (2003) Tissue microenvironments within functional cortical subdivisions adjacent to focal stroke. *J Cereb Blood Flow Metab* 23: 997–1009.
40. Wang L, Zhang Z, Wang Y, Zhang R, Chopp M (2004) Treatment of stroke with erythropoietin enhances neurogenesis and angiogenesis and improves neurological function in rats. *Stroke* 35:1732–1737.
41. Chen P, Goldberg DE, Kolb B, Lanser M, Benowitz LI (2002) Inosine induces axonal rewiring and improves behavioral outcome after stroke. *Proc Natl Acad Sci USA* 99: 9031–9036.
42. Seymour AB, et al. (2005) Delayed treatment with monoclonal antibody IN-1 1 week after stroke results in recovery of function and corticorubral plasticity in adult rats. *J Cereb Blood Flow Metab* 25:1366–1375.
43. Zai L, et al. (2011) Inosine augments the effects of a Nogo receptor blocker and of environmental enrichment to restore skilled forelimb use after stroke. *J Neurosci* 31: 5977–5988.
44. Kleim JA, et al. (2004) Cortical synaptogenesis and motor map reorganization occur during late, but not early, phase of motor skill learning. *J Neurosci* 24:628–633.
45. Kleim JA, Lussnig E, Schwarz ER, Comery TA, Greenough WT (1996) Synaptogenesis and Fos expression in the motor cortex of the adult rat after motor skill learning. *J Neurosci* 16:4529–4535.
46. Holschneider DP, Maarek JM, Yang J, Harimoto J, Scremin OU (2003) Functional brain mapping in freely moving rats during treadmill walking. *J Cereb Blood Flow Metab* 23:925–932.
47. Neeper SA, Gómez-Pinilla F, Choi J, Cotman CW (1996) Physical activity increases mRNA for brain-derived neurotrophic factor and nerve growth factor in rat brain. *Brain Res* 726(1–2):49–56.
48. Liu Z, et al. (2007) Chronic treatment with minocycline preserves adult new neurons and reduces functional impairment after focal cerebral ischemia. *Stroke* 38(1): 146–152.
49. Liu Y, et al. (2009) Overexpression of glycogen synthase kinase 3beta sensitizes neuronal cells to ethanol toxicity. *J Neurosci Res* 87:2793–2802.
50. Wong-Riley M (1979) Changes in the visual system of monocularly sutured or enucleated cats demonstrable with cytochrome oxidase histochemistry. *Brain Res* 171 (1):11–28.
51. Veenman CL, Reiner A, Honig MG (1992) Biotinylated dextran amine as an anterograde tracer for single- and double-labeling studies. *J Neurosci Methods* 41: 239–254.